J Porous Mater (2012) 19:1053–1062
DOI 10.1007/s10934-012-9568-z

Fabrication and high-temperature structural characterization study of porous anodic alumina membranes

K. S. Choudhari · P. Sudheendra · N. K. Udayashankar

Published online: 9 February 2012

Abstract Porous anodic alumina (PAA) membranes with highly ordered array of nanopores were prepared by two-step anodization process. Studies on structural and thermal properties and the thermal stability of the prepared PAA membranes were carried out. Investigation using scanning electron microscopy, atomic force microscopy, X-ray diffraction, thermal analysis and infrared spectroscopy was performed on the prepared PAA membranes at room temperature and in the temperature range 600–1,400 °C. The as-prepared PAA membranes revealed the amorphous nature. Polycrystalline PAA membranes were obtained by annealing carried out at different temperatures. Annealing study confirmed that the heat treatment transformed the amorphous PAA membranes to their crystalline phases, namely, γ-alumina at about 870 °C and then to α-alumina around 1,250 °C.

Keywords Porous anodic alumina membranes · SEM · Thermal analysis · XRD

1 Introduction

Nanoscale materials have been the focus of intense scientific research because of their novel properties and potential applications. One dimensional nanomaterials have gained popularity due to certain unique properties in several fields such as magnetic memories, [1, 2], optoelectronic devices [2], light emitting devices, chemical sensors, microresistors and electrolytic capacitors [3].

In the last two decades, the search for efficient and economic nanomaterial fabrication methods facilitating tunable dimensions and properties, has involved interdisciplinary research and development with emerging technologies in various physical and chemical methods of material preparation. Template assisted synthesis of nanomaterials is an elegant, inexpensive and technologically simple method for the production of nanomaterials. Template synthesis via electrochemical routes offers many incredible advantages over other methods for the production of one-dimensional nanomaterials and ordered porous materials, namely, (i) no need of high temperature, high vacuum or high capital equipments (ii) relatively high growth rate (iii) tuning of the morphology and dimensions of the deposited materials, two or more components can be easily deposited to form multisegmented materials [4]. There are mostly two kinds of templates employed, viz., porous anodic alumina (PAA) and track etched polycarbonate membranes. The excellent mechanical and thermal stability of PAA membranes makes it a perfect candidate for use both as a physical mask [5] for deposition of metallic nanodots catalysts and a supporting template for catalyzed growth of semiconductor nanowires or carbon nanotubes [6, 7]. PAA membranes are a popular choice for the nanomaterial synthesis because of the ease of fabrication of these templates with good control over the pore properties such as pore-diameter and pore-density. PAA membranes possess array of nanopores with the exceptional properties such as high pore density, ideal cylindrical shapes of the pores, controllable pore diameters and

K. S. Choudhari (✉) · N. K. Udayashankar
Department of Physics, National Institute of Technology Karnataka, P.O. Srinivasnagar, Surathkal, Karnataka 575025, India
e-mail: choudhari.k@gmail.com

P. Sudheendra
Department of Metallurgical and Materials Engineering, National Institute of Technology Karnataka, P.O. Srinivasnagar, Surathkal, Karnataka 575025, India

periodicity and a very narrow distribution of pore sizes [8]. These attractive physical properties besides their significant hardness, high thermal and chemical resistance make the PAA membranes suitable for nanomaterial synthesis [9] such as nano-dots, nanowires [10–12] and nanotubes [10, 13, 14] of high aspect ratios, of different materials including metals [1, 15], semiconductors [16, 17] and conducting polymers [9, 18, 19]. PAA membranes are also used widely for biomolecular separations [20] and separations of proteins [21].

In order to spread the applicable fields of PAA membranes further a profound knowledge of their physical properties including their structural and thermal properties at room temperature and at higher temperatures is crucial. Some experimental methods for materials synthesis such as CVD and PVD require high temperature environments and some nanostructures need to be heat treated at high temperature after the fabrication step. Thus the studies on the structural and thermal properties of PAA membranes form an important investigation. In the present work, our objective is to study the structural and thermal properties of the PAA membranes prepared in the laboratory. The thermal stability of the PAA membranes at high temperatures is also investigated. PAA membranes with highly ordered array of nanopores were prepared with varying experimental parameters and their morphological studies were carried out using scanning electron microscopy and atomic force microscopy. The structural and thermal properties of the PAA membranes were investigated using thermal analysis study, X-ray diffraction and infrared spectroscopy.

2 Experimental

The PAA membranes with highly ordered arrangement of nanopores arrays were prepared by two-step anodization. Prior to anodization, high purity aluminium foils (Merck, thickness 0.3 mm) were degreased in acetone for 1 h followed by 20 min of ultrasonic cleaning. Then, the samples were annealed at 500 °C for 5 h in vacuum. The samples were rinsed with double distilled water and then etched in 2.0 mol/l NaOH at 50 °C to remove the natural oxide present on the surface. The samples were then dipped in 1.5 mol/l nitric acid for $\sim$3 min to counteract the remnant lye. After rinsing with double distilled water again, the specimens were electrochemically polished at 200 mA/cm^2 in a mixture of concentrated chromic and phosphoric acids (2:8) for 8 min, rinsed in running double distilled water and finally dried in the warm air stream. Anodization process was carried out in 0.3 M oxalic acid, 0.3 M sulfuric acid and 10 wt% phosphoric acid solutions at various anodization potentials. The temperature of the solution was maintained at about 5 °C. A two-electrode configuration was used with the electropolished aluminium sample as anode and a cleaned aluminium sheet, of the same area as that of the anode, as cathode. A constant stirring of the electrolyte was maintained throughout the experiments. The duration of the first stage anodization was 2 h. The formed PAA layer was then removed by immersing the specimen in a mixture of 1.8 wt% chromic acid and 6 wt% phosphoric acid at 60 °C for 2 h. Subsequent step of second stage anodization was carried out under the same condition as the first step, with the duration of 2 h. Pore widening is usually performed after the second anodization step using phosphoric acid solution for desired time period to achieve the required pore dimensions. A 5 wt% phosphoric acid solution was used for pore widening of the prepared PAA membranes. Pore widening was performed for 30, 45 and 60 min.

The studies on surface morphology of the prepared PAA membranes were carried out using JEOL/JSM—6380LA, Analytical Scanning Electron Microscope, Raith e Line and Carl Zeiss Ultra 55 FESEM. Atomic force microscopy imaging for topography was carried out using Agilent 5500 AFM. X-ray diffraction studies were carried out using JEOL Model- DX-GE-2P, X-ray diffractometer with Cu Kα radiation ($\lambda = 1.5418$ Å), acceleration voltage of 20 kV, working current of 30 mA, step angle of 0.02° over the scan range 20°–90° at a scanning rate of 2°/min. Thermal characterization for Thermogravimetric (TG) and Differential thermal analysis (DTA) of PAA membrane samples were carried out using Exstar 6000 TG/DTA 6300 Thermal analyzer in nitrogen atmosphere at a heating rate of 10 K/min. Fourier transform infrared spectra were recorded using Thermo Scientific NICOLET 6700.

3 Results and discussion

Prior to anodization experiments the aluminum substrates were electropolished to reduce the roughness of the metals surfaces. The substrates after electropolishing appear smooth and shiny with the lustrous mirror finish. Figure 1 shows the optical images of the top surfaces of the aluminum substrates before (Fig. 1a) and after (Fig. 1b) electropolishing. These electropolished substrates were used for anodization. Figure 2a shows the electron micrograph of the PAA membrane obtained after the first step anodization. During the first step, the pores usually nucleate at random positions, and hence the pores on the surface are irregular and have a broad distribution. The substrate, after removing the disordered pore structure using wet chemical etching, appears as shown in Fig. 2b where the self-organized, closely packed concave dimples over the sample's surface can clearly be seen. After the

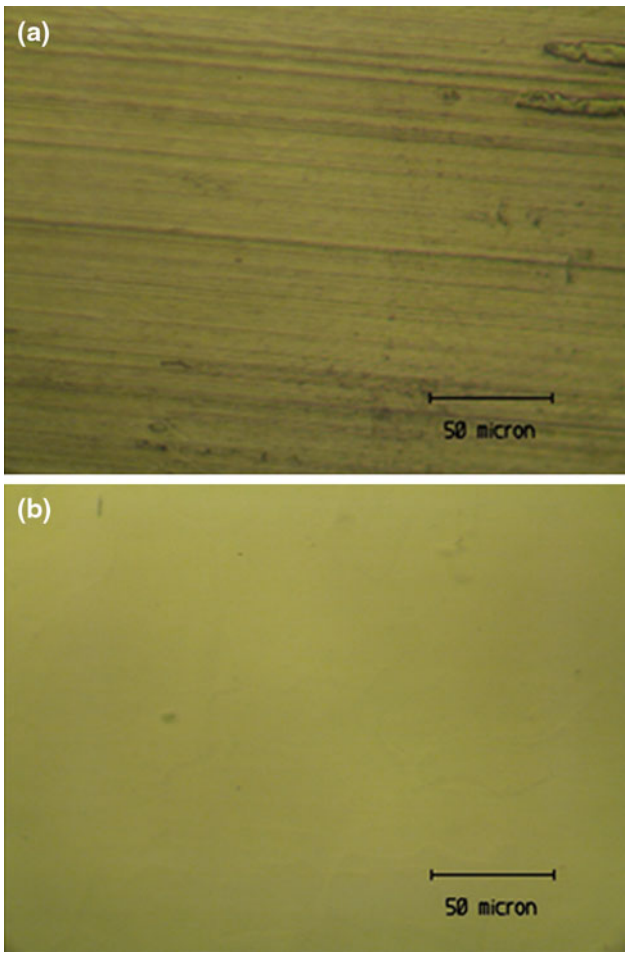

Fig. 1 The top surface optical images of aluminum substrates used for preparation of PAA membranes: **a** the rough surface of the substrate showing the scales on it before the electropolishing and **b** view of the same surface after electropolishing

second step anodization well-ordered and hexagonally arranged pores were obtained as shown in Fig. 2c and d.

Figure 3 shows the AFM images of PAA membranes prepared in 0.3 M oxalic acid at 40 V (Fig. 3a) and 10 wt% phosphoric acid solution at the anodization potentials of 90 V (Fig. 3b), 120 V(Fig. 3c) and 150 V(Fig. 3d). The PAA membranes prepared with 40 V show well ordered, hexagonally arranged pore arrays whereas this type of regular arrangement is not observed for other voltage values. It has been observed that the best periodic arrangements can be obtained at 40 V for membranes prepared in oxalic acid solution and at 160 V for those prepared in phosphoric acid solution [22]. Hence significant ordering was not observed in the case of membranes prepared at 90 and 120 V. However a small amount of ordering in the arrangement of pores was observed in the membranes prepared with 150 V. In an AFM image the black portions correspond to the pores and the center of the pores can be identified by the troughs or valleys in the line profile of the corresponding AFM image. It is well known that the interpore distance of PAA membranes depend on the applied anodization potential. The interpore distances were determined by the line profiles by measuring the separation between two adjacent valleys (markers are shown in the figure). Measurements of interpore distance on SEM images were also carried out and the results along with the AFM results are shown in Table 1. It can be seen that the interpore distance values from both the microscopies matched very well.

Figure 4 shows the electron microscopic images of PAA membranes prepared in 0.3 M oxalic acid at 40 V subjected to pore widening. Figure 4a, b and c show the surface view of the membranes after the pore widening was performed for 30, 45 and 60 min, respectively. PAA membranes obtained by two-step anodization in 0.3 M oxalic acid at 40 V and without any pore widening are shown in Fig. 2c and d. The pore widening process increases the pore-diameters of the PAA membranes. The wall thickness of the pores decreases as the pore widening time increases. However, it is observed that there is no change in the interpore distance with the pore widening process.

The structural features of the PAA membranes, viz., pore diameters, interpore distance, porosity and pore density were calculated using ImageJ-image analysis software (ImageJ) and also using the relationships [23, 24]:

$$D_i = k \cdot U \tag{1}$$

$$D_p = \sqrt{\frac{2\sqrt{3} \cdot P}{\pi}} \cdot D_i \tag{2}$$

where, D_i is the interpore distance, k is the proportionality constant with the value of 2.5 $\mathrm{nmV^{-1}}$, U is the anodization potential, D_p is the pore diameter and P is the porosity. Also,

$$P = \frac{\pi}{2\sqrt{3}} \cdot \left(\frac{D_p}{D_i}\right)^2 \tag{3}$$

$$n = \frac{2 \times 10^{14}}{\sqrt{3} \cdot D_i^2} \tag{4}$$

where, n is the pore density, defined as the number of pores per square cm.

The structural characterization data of PAA membranes including pore diameter, interpore spacing, porosity and pore density is displayed in Table 2. It is observed that the results from both the SEM images (manual measurements) and ImageJ agree very well and are also consistent with the literature values. Images used for this analysis were of different magnifications. The pore diameters and the porosity values both show an increasing trend with the increase in the pore widening time. On the other hand,

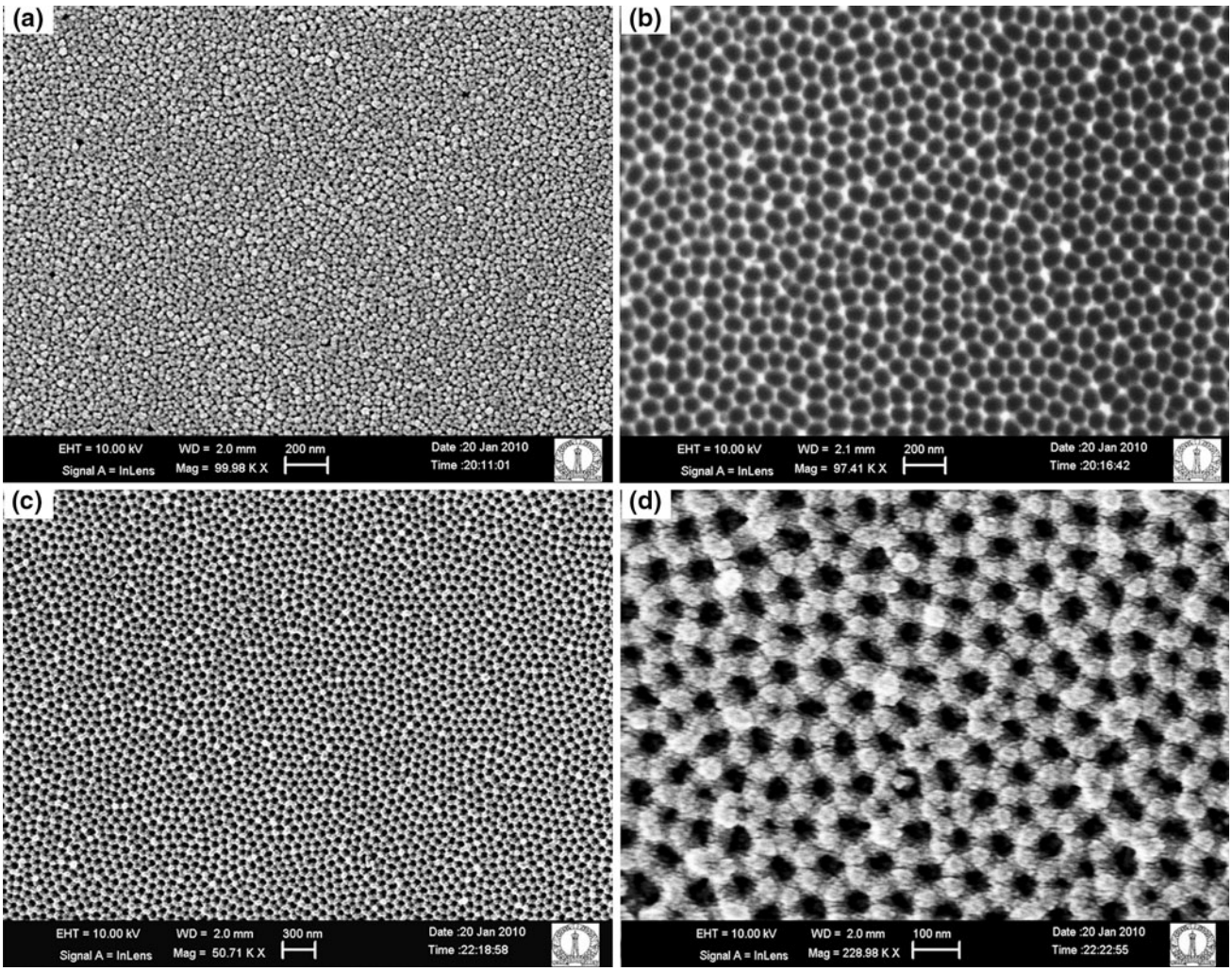

Fig. 2 FESEM images of the samples prepared by anodization in 0.3 M oxalic acid at 40 V. **a** First step anodized sample, **b** substrate surface showing the concave dimples after removing the disordered pores of first step by chemical etching, **c** PAA membrane after two-step anodization process and d magnified view of the surface of the PAA membrane

interpore distance and pore density values are constant as these properties are dependent on applied voltage.

As prepared nanoporous anodic alumina membranes were amorphous in phase as shown in Fig. 5. Independent anodic alumina separated from the substrate was characterized by X-Ray Diffraction (XRD) and the obtained pattern is shown in Fig. 5a. Intact aluminum oxide, not separated from the substrate is also subjected to XRD and the diffractogram is shown in Fig. 5b. The diffraction pattern of the alumina with substrate shows the amorphous nature of the alumina along with the peaks corresponding to the aluminum substrate and match with the JCPDS data (85-1327).

Annealing of the prepared alumina membranes were carried out to study the effect of heat treatment on their structures. In order to find the crystallization temperature, thermogravimetric analysis was carried out. Thermogravimetric analysis (TGA) can be used to reveal the changes in the anodic alumina membrane during the process of annealing. Figure 6 shows the TGA curve of the as-prepared alumina membrane formed in oxalic acid solution electrolyte. The mass loss in the curve from room temperature to about 400 °C is ca. 2.65% and is attributed to the dehydration process i.e. desorption of weakly bound water from the surface and the inner walls of the nanopores. In the second region of temperature from 400 to about 510 °C the mass loss is about 0.25% and may be from the decomposition of oxalic impurities because the decomposition of metal oxalates is believed to occur at temperature higher than 350 °C [25]. At about 870 °C a strong phase transition is observed. In accordance with the corresponding XRD patterns it can be observed that this transition is the transformation of amorphous alumina to γ-alumina [26]. During this transformation the –OH groups in the crystalline structure of

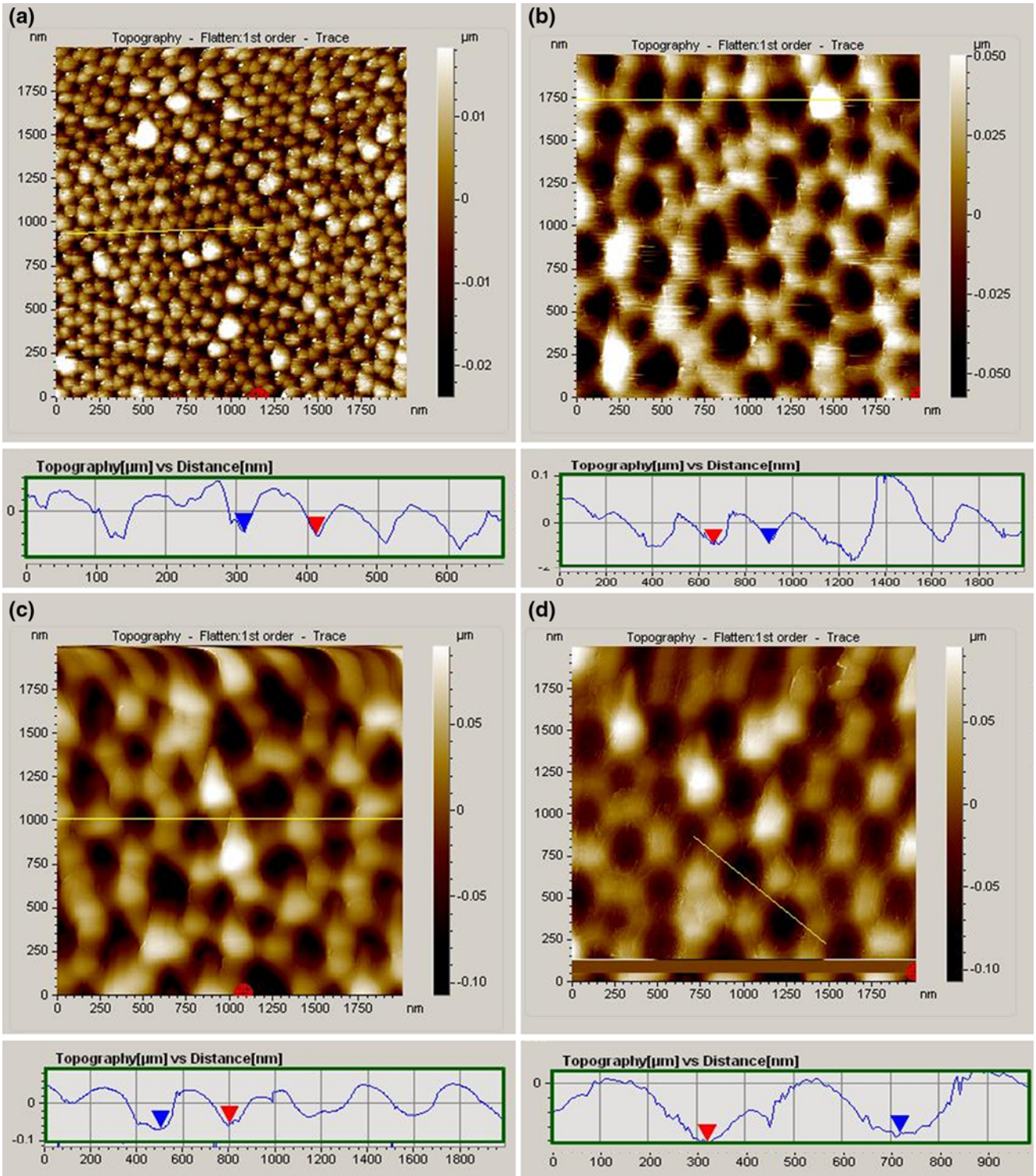

Fig. 3 AFM images of PAA membranes, showing topography and the line profiles, prepared in **a** oxalic acid solution at the anodization potential of 40 V; and in phosphoric acid solution at voltages **b** 90 V, **c** 120 V and **d** 150 V

γ-Al_2O_3 will be lost [27] and this is the thermal decomposition of the dopant species (the oxalate groups present in the alumina prepared in the oxalic acid) which results in the weight loss (about 7%).

Fig. 7 presents the X-ray diffractograms of the as-prepared nanoporous anodic alumina and alumina annealed at different temperatures for 1 h duration. The as-prepared alumina is amorphous in nature. No crystallinity was

Table 1 Interpore distances of PAA membranes determined from SEM and AFM images

Sample name	Voltage (V)	Interpore distance	
		SEM (nm)	AFM (nm)
AA49	40	92.7	101.4
AA26	90	247.3	253.4
AA86	120	325.6	320.9
AA150	150	395.3	395.3

detected as the temperature was raised up to 800 °C. Beyond this temperature the amorphous phase of alumina starts transforming into γ-alumina phase. The diffraction pattern of sample annealed at 900 °C shows mainly two diffraction peaks at $2\theta = 45.32°$ and 67.04° which match very well with that of γ-Al_2O_3 (JCPDS, 10-0425). As the temperature increased to 1,000 °C it was found that diffraction peaks corresponding to both α and γ phases are present. The peaks at around 38.0° and 43.1° correspond to α-alumina whereas the peaks of 45.32° and 67.04° are from γ-alumina as were observed in 900 °C pattern. At 1,100 °C there are several peaks in the pattern belonging to α phase. The peaks at about 45° and 67° have disappeared and 8 new peaks were observed at 25.7°, 35.28°, 37.98°, 43.42°, 52.62°, 57.56°, 66.64°, and 68.24° which belong to α-Al_2O_3 (JCPDS, 42-1468). The initial crystallization and the phase transformation of the membranes can be confirmed by their mechanical properties. With heat treatment the alumina membranes lose their flexibility and there is an increase in their fragility and tendency of breaking at higher temperature heat treatment. The decrease in flexibility takes place sharply in the course of reorganizations of oxide lattice particularly when phase transitions from amorphous to polycrystalline γ-Al_2O_3 and in turn to α-Al_2O_3 takes place. We have observed that the α-Al_2O_3 phase is so fragile that it can not be used for routine practical applications of membranes, similar to the observations of Mardilovich et al. [28]. Brown et al. [29] discussed that the thermal events that take place in membranes during heat treatment are irreversible on thermal cycling and hence confirm the permanent structural changes within the membranes. Also Xu et al. [30] confirmed the α-Al_2O_3 phase of alumina membranes, which were heat treated at 1,100 °C, with the help of micro-Raman spectrum. Hence the heat treatment study clearly reveals that the structural transition from amorphous to γ phase and in turn to α phase can be realized in nanoporous anodic alumina through different high-temperature annealings.

The initial composition of the as-formed nanoporous anodic alumina is not pure Al_2O_3. A considerable amount of anionic impurities or hydroxyl groups are found in the

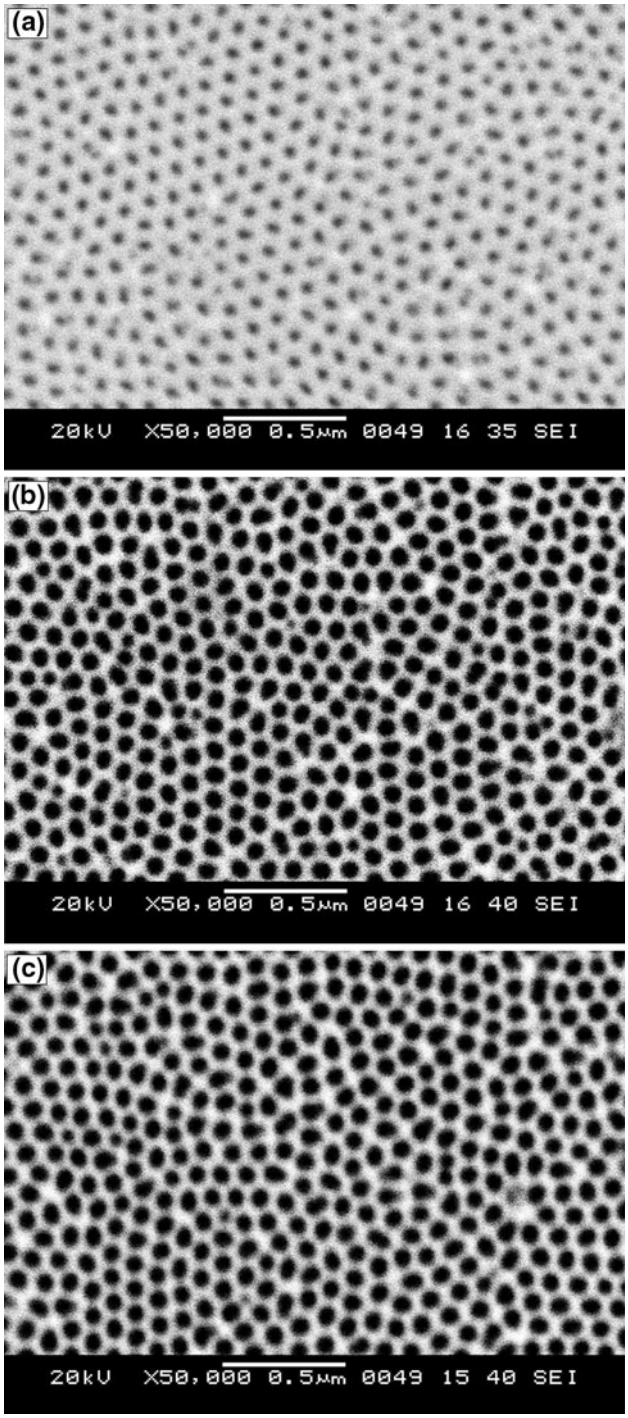

Fig. 4 SEM images of PAA membranes prepared in 0.3 M oxalic acid at 40 V and pore widened by chemical etching in 5 wt% phosphoric acid solution for **a** 30 min, **b** 45 min and **c** 60 min

alumina structure or get bound on the surface, which come from the electrolyte used for the alumina preparation. Room temperature infrared transmission spectra of the as prepared alumina and alumina annealed at different temperatures are shown in Fig. 8. The broad absorption band of 2,800–3,700 cm^{-1} can be attributed to H_2O molecular

Table 2 Structural characterization data of PAA membranes, using electron microscopy (SEM) images and the software-ImageJ, for various durations of the pore widening carried out in 5 wt% H_3PO_4 at room temperature

Sample	Time (min)	Magnification (×)	Interpore distance (nm)		Pore diameter (nm)		Porosity (%)		Pore density $\times 10^{10}$ (cm^{-2})	
			SEM	ImageJ	SEM	ImageJ	SEM	ImageJ	SEM	ImageJ
AA4902	0	228k	101 ± 9	104 ± 11	46 ± 4	47 ± 5	18.4	17.0	1.02	1.14
AA4903		520k	100 ± 11	101 ± 11	45 ± 6	45 ± 5			1.06	1.19
AA19506	30	50k	102 ± 9	103 ± 8	53 ± 4	49 ± 4	24.6	22.8	1.01	0.89
AA19507		100k	103 ± 7	100 ± 6	54 ± 7	53 ± 4			1.02	0.88
AA19605	45	30k	102 ± 7	103 ± 8	63 ± 5	65 ± 5	35.1	37.0	1.01	0.86
AA19609		80k	102 ± 8	100 ± 5	64 ± 4	64 ± 4			1.03	0.96
AA19706	60	40k	103 ± 7	101 ± 9	71 ± 5	73 ± 6	43.5	46.1	1.03	0.92
AA19709		100k	102 ± 9	101 ± 11	71 ± 5	71 ± 4			1.03	0.93

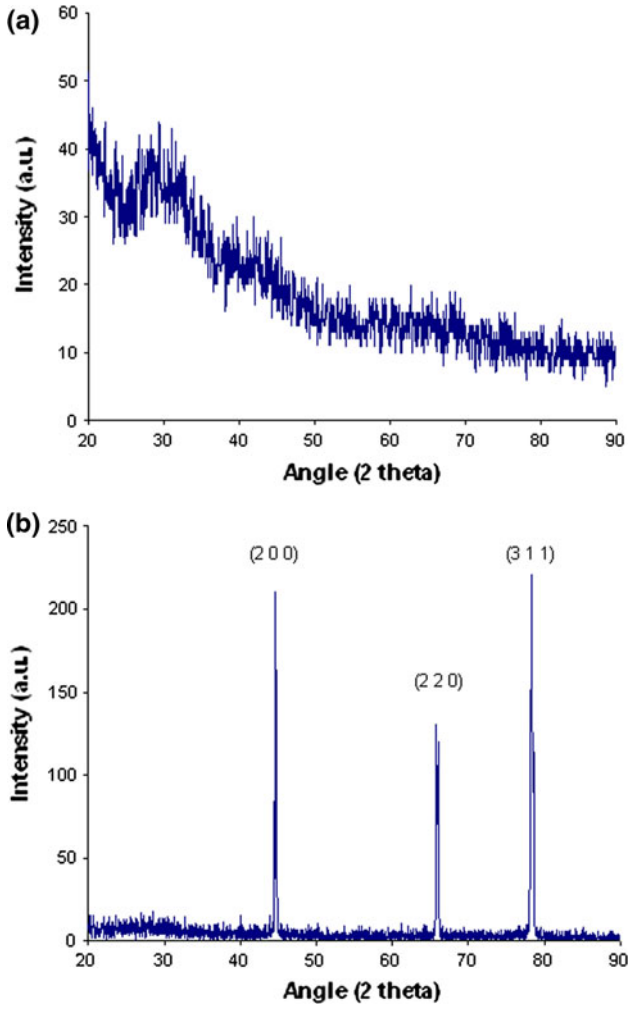

Fig. 5 X-ray diffractogram of the as prepared nanoporous anodic alumina **a** independent nanoporous anodic alumina membrane and **b** alumina on the substrate

and/or—OH stretching vibrations. The arising of a sharp peak at 2,342 cm^{-1} showing variation in intensity along with the different annealing temperatures is attributed to the formation of CO_2 inside the alumina films. During the heat treatment a fraction of the oxalic impurities get carbonized and remainders get converted to CO_2. The peak starts growing with temperature and reaches its maximum at 700 °C and starts reducing then on. The alumina heat treated at 700 °C is still amorphous with largest amount of oxalic impurities converted into CO_2 trapped into the alumina. With further increase in the temperature the intensity of the peak reduces and this can be related to the amorphous phase changing to γ-alumina phase [31]. The infrared absorption peaks at 1,460 and 1,580 cm^{-1} can be attributed to the two possible C–O bonds in the oxalate ion structure. The intensity of these peaks reduces as the annealing temperature is raised.

There are significant physical changes in the PAA membranes upon heating. The prepared PAA membranes which are planar at room temperature commence to curling up or rolling up into a tubular structure at the temperature of about 800 °C and higher. This type of curling behavior is well known in heated ceramic systems [29]. There may be a possibility of destruction of the nanostructures of PAA membranes upon heating. The SEM images showing the surface morphologies of the PAA membranes prepared in sulfuric acid solution without heat treatment and with heat treatment at 1,000 and 1,200 °C are shown in Fig. 9. It can be seen in Fig. 9b that there is no apparent change in the nanostructures of the membranes when heated at 1,000 °C. Similar observations were reported by Brown et al. [29]. Some cracks were observed by Fernandez-Romero et al. [32] when alumina membranes were heat treated at 1,100 °C. In another study Yang et al. [33] reported that there is no noticeable change in the nanostructures of the alumina membranes heated at 1,220 °C. Whereas, in contrast to this, we observed that there is a small amount of cracks or breakages of the pore walls in the membranes as can be seen in Fig. 9c. It has been observed that the pore walls of few pores break at random places throughout the membrane and merge with the neighboring pores. Thus it

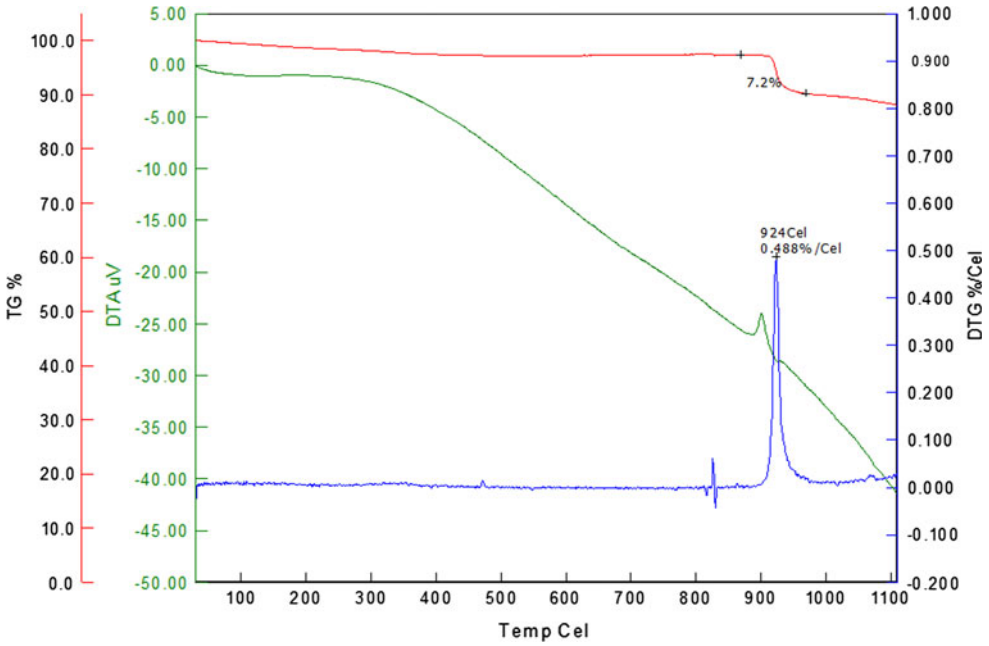

Fig. 6 Thermogravimetric analysis curve for the as-prepared anodic alumina

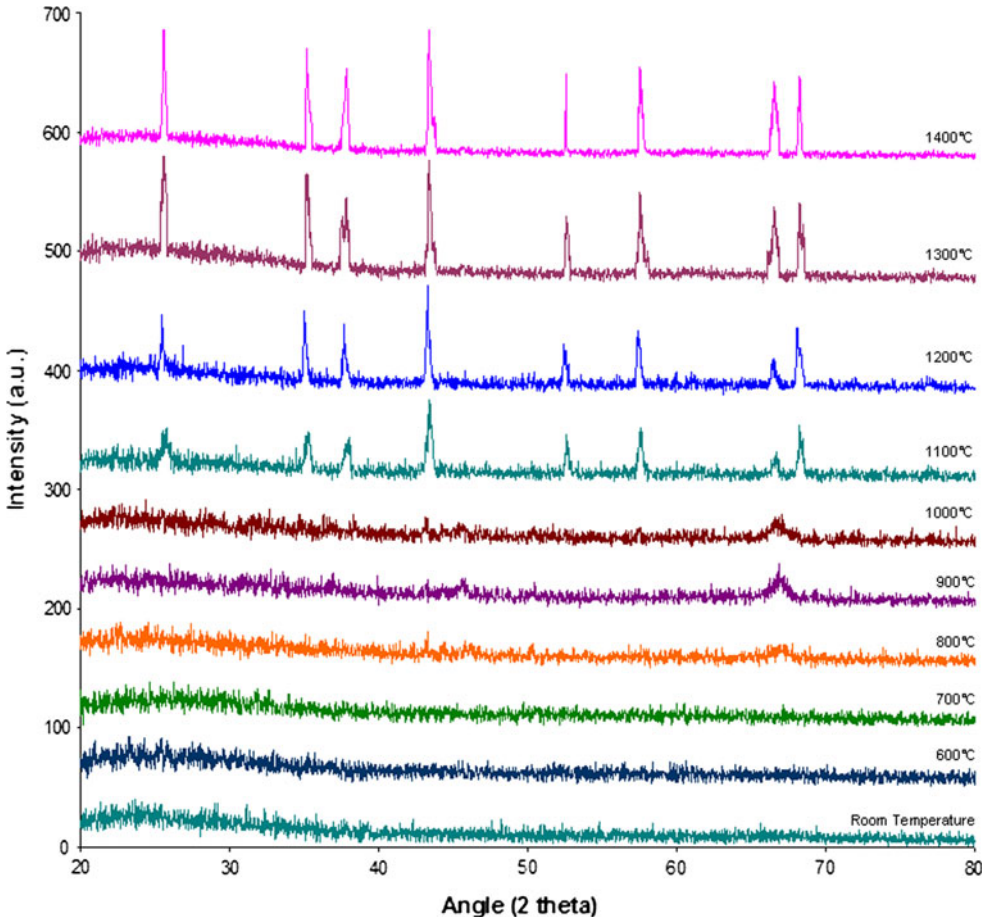

Fig. 7 XRD patterns of the as prepared nanoporous anodic alumina and the anodic alumina annealed at different temperatures in atmosphere for 1 h. The *curves* have been shifted in the *y*-axis for clarity sake

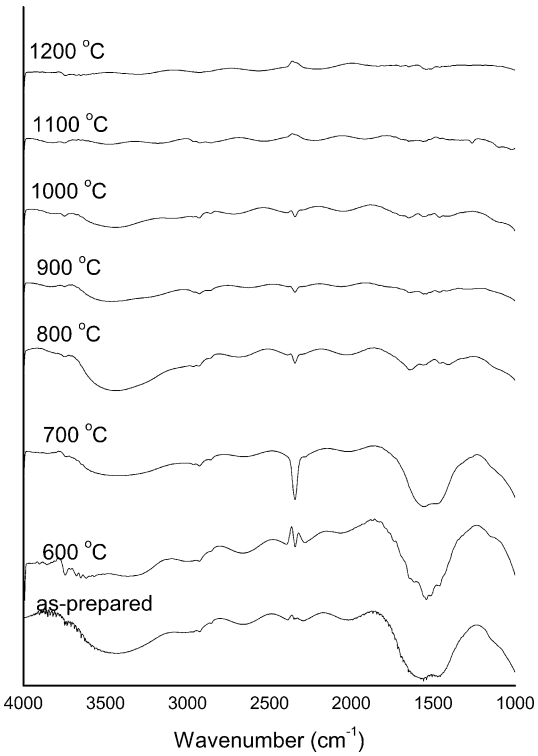

Fig. 8 Infrared transmission spectra of the as-prepared nanoporous anodic alumina and alumina annealed at different temperatures for 1 h. The *curves* have been shifted in the *y*-axis for clarity sake

can be concluded that the PAA membranes maintain a significant thermal stability when heated up to 1,000 °C and lose the stability of the nanostructures beyond 1,200 °C.

4 Conclusions

PAA membranes with highly ordered nanopores array were prepared at different anodization voltages. The membranes prepared in oxalic acid were pore-widened in 5 wt% phosphoric acid solution for different durations and the progress of the pore widening process was investigated. The structural and thermal analysis of the PAA membranes carried out at room temperature and in the temperature range 600–1,400 °C indicated that the as-prepared membranes are amorphous. Thermal stability studies of the PAA membranes indicated that there was no apparent change in the morphology of the PAA membranes when heated at temperatures of up to 1,000 °C. However, there is a small amount of destruction of the nanostructures of PAA membranes when heated beyond 1,200 °C. In accordance with the thermal analysis and X-ray diffractogram analysis it is evident that the as-prepared PAA membrane which is amorphous at room temperature can be transformed to crystalline γ-Al_2O_3 phase by carrying out the heat treatment at the temperature above 870 °C. At the temperature of about 1,250 °C the γ-Al_2O_3 gets transformed to α-Al_2O_3.

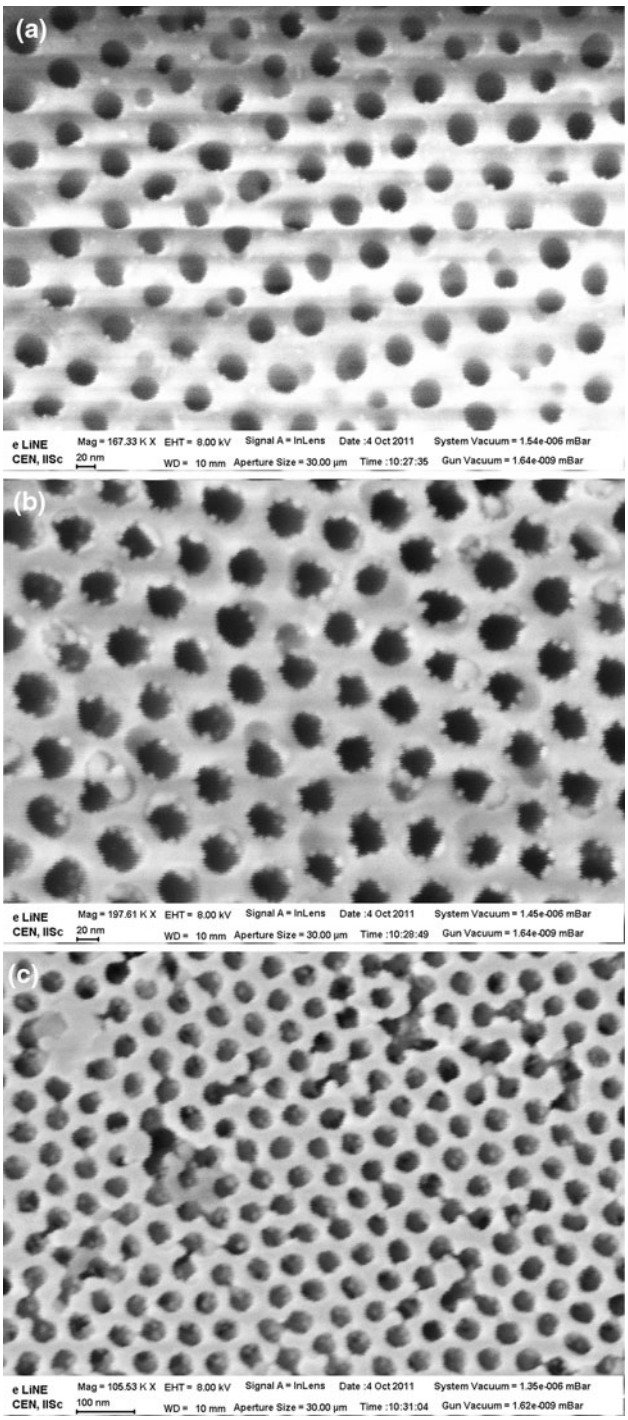

Fig. 9 SEM images of the as-prepared and heat treated PAA membranes prepared in sulfuric acid solution at 25 V, **a** surface view of the as-prepared PAA membrane and heat treated membranes at **b** 1,000 °C and **c** 1,200 °C

Acknowledgments K. S. Choudhari (KSC) gratefully acknowledges the Indian Nanoelectronics Users Program (INUP) at Centre of Excellence in Nanoelectronics (CEN), Indian Institute of Science (IISc), Bangalore, through which the SEM, AFM and FTIR facilities were made available. KSC is grateful to Dr. S. Venugopal and Mr. M. Girish of Department of Chemical Engineering, Indian Institute of Science, Bangalore for providing FESEM facility. KSC is thankful to NITK Surathkal for the award of a Research Fellowship.

References

1. H. Masuda, K. Fukuda, Science **268**, 1466 (1995)
2. J. Zhou, J. He, G. Zhao, C. Zhang, J. Zhao, H. Hu, Trans. Nonferrous Met. Soc. China **17**, 82 (2007)
3. A. Mozalev, A. Mozaleva, M. Sakairi, H. Takahashi, Electrochim. Acta **50**, 5065 (2005)
4. M. Lai, D.J. Riley, J. Colloid, Interf. Sci. **323**, 203 (2008)
5. Z. Chen, Y. Lei, H.G. Chew, L.W. Teo, W.K. Choi, W.K. Chim, J. Cryst. Growth **268**, 560 (2004)
6. W.Y. Jang, N.N. Kulkarni, C.K. Shih, Z. Yao, Appl. Phys. Lett. **84**, 1177 (2004)
7. J. Li, C. Papadopoulos, J.M. Xu, M. Moskovits, Appl. Phys. Lett. **75**, 367 (1999)
8. S. Thongmee, H.L. Pang, J. Ding, J.Y. Lin, J. Magn. Magn. Mater. **321**, 2712 (2009)
9. Y. Ren, Q.F. Liu, S.L. Li, J.B. Wang, X.H. Chan, J. Magn. Magn. Mater. **321**, 226 (2009)
10. L.F. Marsal, L. Vojkuvka, P. Formentin, J. Pallares, J. Ferre-Borrull, Opt. Mater. **31**, 860 (2009)
11. Z. Zhang, D. Gekhtman, M.S. Dresselhaus, J.Y. Ying, Chem. Mater. **11**, 1659 (1999)
12. G. Sauer, G. Brehm, S. Schneider, K. Nielsch, R.B. Wehrspohn, J. Choi, H. Hofmeister, U. Gosele, J. Appl. Phys. **91**, 3243 (2002)
13. Z.L. Xiao, C.Y. Han, U. Welp, Nano Lett. **2**, 1293 (2002)
14. M. Steinhart, J.H. Wendorff, A. Greiner, R.B. Wehrspohn, K. Nielsch, J. Schilling, J. Choi, U. Gosele, Science **296**, 197 (2002)
15. J. Qin, J. Chem. Mater. **17**, 1829 (2005)
16. Z. Miao, D.S. Xu, J.H. Ouyang, J. Nano Lett. **2**, 717 (2002)
17. M.S. Sander, R. Gronsky, T. Sands, A.M. Stacy, Chem. Mater. **15**, 335 (2003)
18. C.W. Wang, Z. Wang, M.K. Li, H.L. Li, Chem. Phys. Lett. **341**, 431 (2001)
19. A. Belwalkar, E. Grasing, W.V. Geertruyden, Z. Huang, W.Z. Misiolek, J. Membr. Sci. **319**, 192 (2008)
20. H.U. Osmanbeyoglu, T.B. Hur, H.K. Kim, J. Membr. Sci. **343**, 1 (2009)
21. J.L. Snyder, A. Clark Jr, D.Z. Fang, T.R. Gaborski, C.C. Streimer, P.M. Fauchet, J.L. McGrath, J. Membr. Sci. **369**, 119 (2011)
22. A.P. Li, F. Muller, A. Birner, K. Nielsch, U. Gosele, J. Appl. Phys. **84**, 6023 (1998)
23. K. Nielsch, J. Choi, K. Schwirn, R.B. Wehrspohn, U. Gosele, Nano Lett. **2**, 677 (2002)
24. G.D. Sulka, A. Brzozka, L. Zaraska, M. Jaskula, Electrochim. Acta **55**, 4368 (2010)
25. X. Sun, F. Xu, Z. Li, W. Zhang, J. Lumin. **121**, 588 (2006)
26. P. Bocchetta, C. Sunseri, G. Chiavarotti, F.D. Quarto, Electrochim. Acta **48**, 3175 (2003)
27. M.E. Mata-Zamora, J.M. Saniger, Rev. Mex. Fıs. **51**, 502 (2005)
28. P.P. Mardilovich, A.N. Govyadinov, N.I. Mukhurov, A.M. Rzhevskii, R. Peterson, J. Member, Science **98**, 131 (1995)
29. I.W.M. Brown, M.E. Bowden, T. Kemmitt, K.J.D. MacKenzie, Curr. Appl. Phys. **6**, 557 (2006)
30. W.L. Xu, M.J. Zheng, S. Wu, W.Z. Shen, Appl. Phys. Lett. **85**, 4364 (2004)
31. X.H. Wang, C.Y. Li, G. Chen, L. He, H. Cao, Appl. Phys. A **98**, 745 (2010)
32. L. Fernandez-Romero, J.M. Montero-Moreno, E. Pellicer, F. Peiro, A. Cornet, J.R. Morante, M. Sarret, C. Muller, Mater. Chem. Phys. **111**, 542 (2008)
33. S.G. Yang, T. Li, L.S. Huang, T. Tang, J.R. Zhang, B.X. Gu, Y.W. Du, S.Z. Shi, Y.N. Lu, Phys. Lett. A **318**, 440 (2003)